Supporting Information

2D ultrathin surfactant-encapsulating polyoxometalate assemblies as carriers for monodispersing noble-metal nanoparticles with high catalytic activity and stability

Xing-Yu Ji[a], Fei-Yang Yu[a], Ying-Qi Li[a,*], Hao-Tian Zhu[a], Hui-Ying Zhao[a], Yue Shi[a], Yong-Hui Wang[a,*], Hua-Qiao Tan[a] and Yang-Guang Li[a,*]

Key Laboratory of Polyoxometalate Science of Ministry of Education, Faculty of Chemistry, Northeast Normal University, Changchun, 130024, P. R. China.

E-mail: andyli24@outlook.com; wangyh319@nenu.edu.cn; liyg658@nenu.edu.cn

Postal address: Northeast Normal University, Renmin Street No. 5268, Changchun, Jilin Province, 130024, P. R. China

Chemicals and Reagents

Dimethyldioctadecylammonium bromide (DODA·Br), phosphomolybdic acid ($H_3PMo_{12}O_{40}$), sodium oleate (chemically pure), silver nitrate ($AgNO_3$), 4-nitrophenol (4-NP), sodium borohydride ($NaBH_4$), chloroform ($CHCl_3$), *n*-butanol (*n*-buOH) and isopropanol (IPA) were purchased commercially. All chemicals and organic solvents were of analytical reagent grade and used as received without any further purification.

Characterization Methods.

Fourier Transform Infrared spectra (FTIR) was derived from Perkin Elmer Fourier Transform Infrared Spectrometer GX. The UV/Vis absorption spectra was measured on a UV-7502PC UV/Vis spectrophotometer at room temperature. The UV-Vis diffuse reflectance spectra (DRS) measurements were received by a UV-2600 UV-Vis spectrophotometer (Shimadzu), and $BaSO_4$ was employed as a background. The powder X-ray diffraction (PXRD) measurements were recorded on a Bruker AXS D8 Focus using filtered Cu K_α radiation (λ=1.54056 Å). X-ray photoelectron spectra (XPS) was employed to analyze elements P, Mo, and Ag, which were analyzed on an ESCALAB 250 spectrometer (Thermo Electron Corp.) with Al K_α radiation ($h\upsilon$ = 1486.6 *e*V) as the excitation source. The surface morphology of the materials has been performed on a JEOL JSM 4800F SEM. The transmission electron microscopy (TEM) and HRTEM images were carried out on a JEM-2100F microscope at an acceleration voltage of 200 kV. The corresponding energy dispersive X-ray detector (EDX) spectra were recorded on a SU8000 ESEM FEG microscope. The ICP-AES elemental analysis was performed on a Prodigy Leeman ICP-AES spectrometer. The size distribution statistics of Ag NPs were calculated by sampling 50 points in the SEM images using the software (Nano measurer). Atomic force microscope (AFM) measurement was carried out on Dimension ICON instrument (Busker). Dynamic Light Scattering (DLS) analysis was performed using a Zetasizer Nano S (Malvern Panalytical).

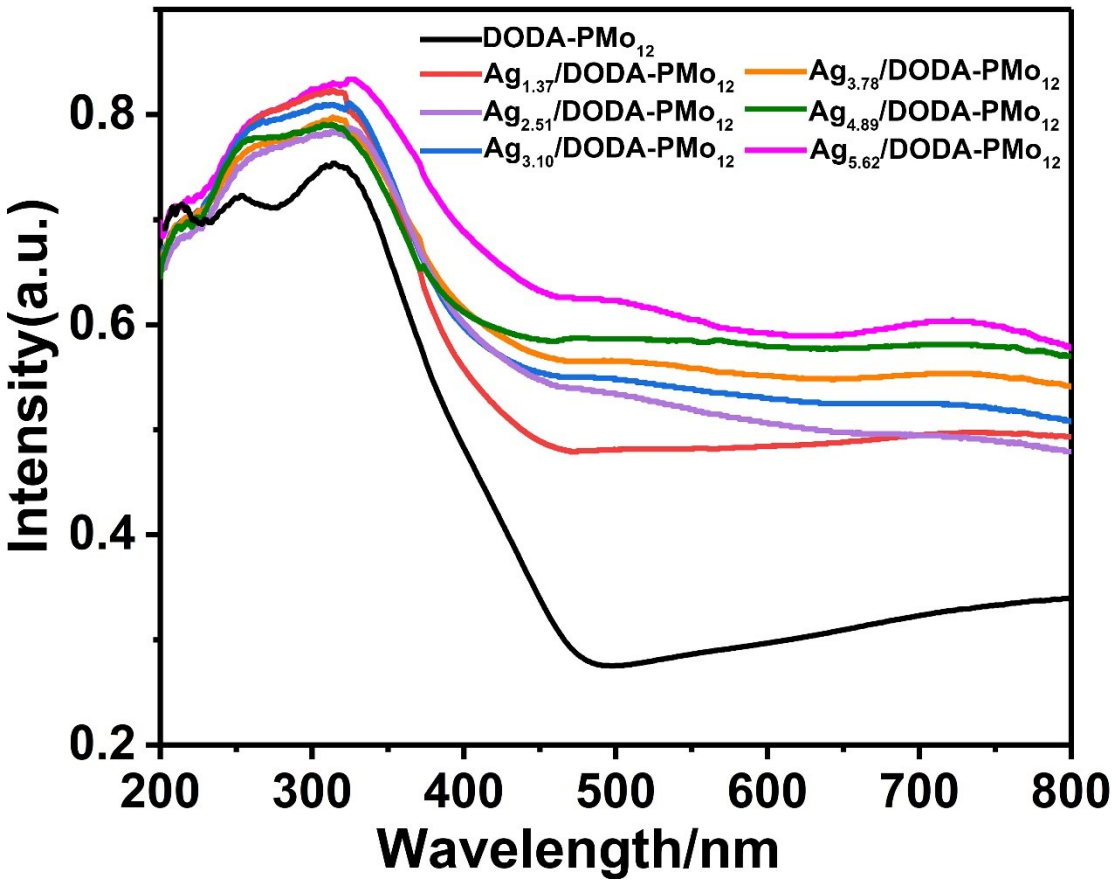

Figure S1. UV-vis diffuse reflectance spectra of DODA-PMo_{12} and Ag/DODA-PMo_{12} composites with different loading amount of Ag NPs, 1.37wt%, 2.51wt%, 3.10wt%, 3.78wt%, 4.89wt% and 5.62wt%.

The UV-vis spectra of the DODA-PMo_{12} and Ag/DODA-PMo_{12} composites with different loading amount of Ag NPs were measured by the UV-vis diffuse reflectance spectra in the range of 200-800 nm. For Ag/DODA-PMo_{12} composites, a wide absorption peak at about 480 nm has been clearly observed, which can be attributed to the surface plasmon resonance (SPR) absorption of Ag NPs. With the increase of the loading amount of Ag NPs, the absorption bands were enhanced.

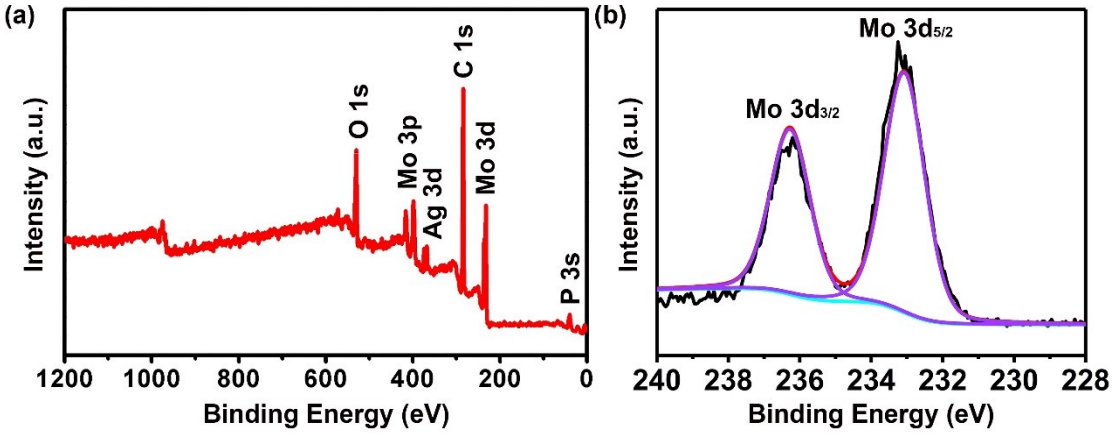

Figure S2. (a) The full scan survey XPS spectrum of Ag/DODA-PMo_{12} composite. (b) Mo 3*d* electrons of $H_3PMo_{12}O_{40}$.

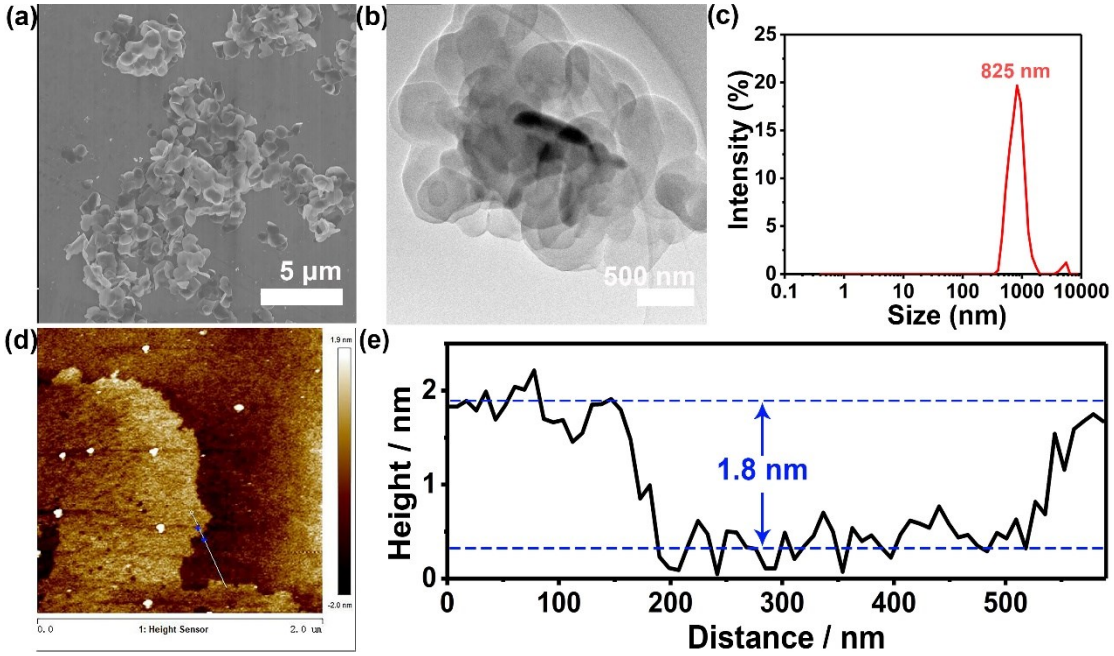

Figure S3. (a) SEM image，(b) TEM image，(c) Scattering intensity and particle number distribution curves, (d) AFM image and (e) the corresponding height profile of DODA-PMo_{12}.

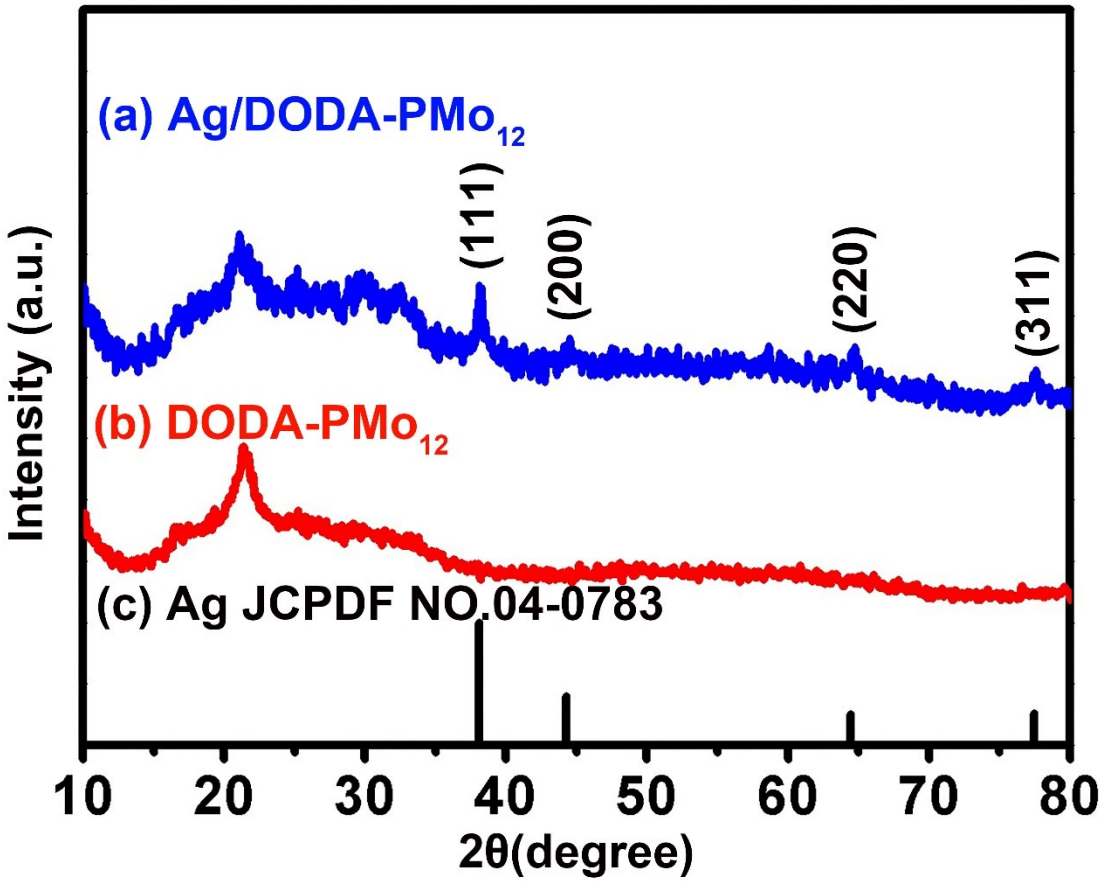

Figure S4. Wide-angle XRD patterns of (a) Ag/DODA-PMo_{12} composite, (b) DODA-PMo_{12} and (c) JCPDF No. 04-0783 of metallic Ag.

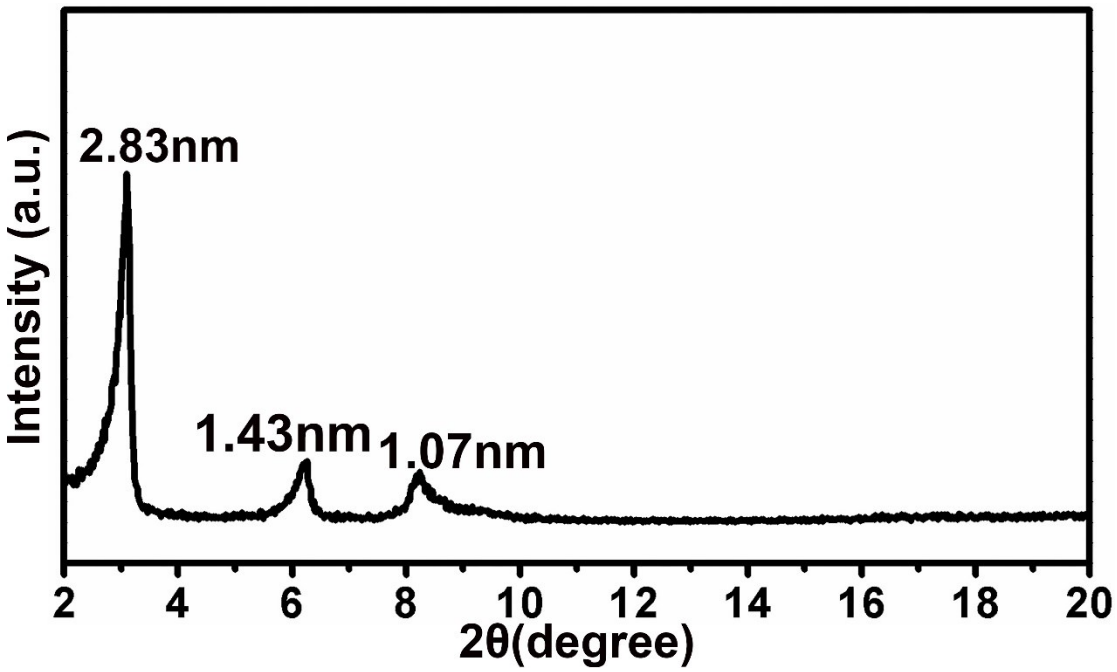

Figure S5. Small-angle XRD pattern of Ag/DODA-PMo_{12} composite.

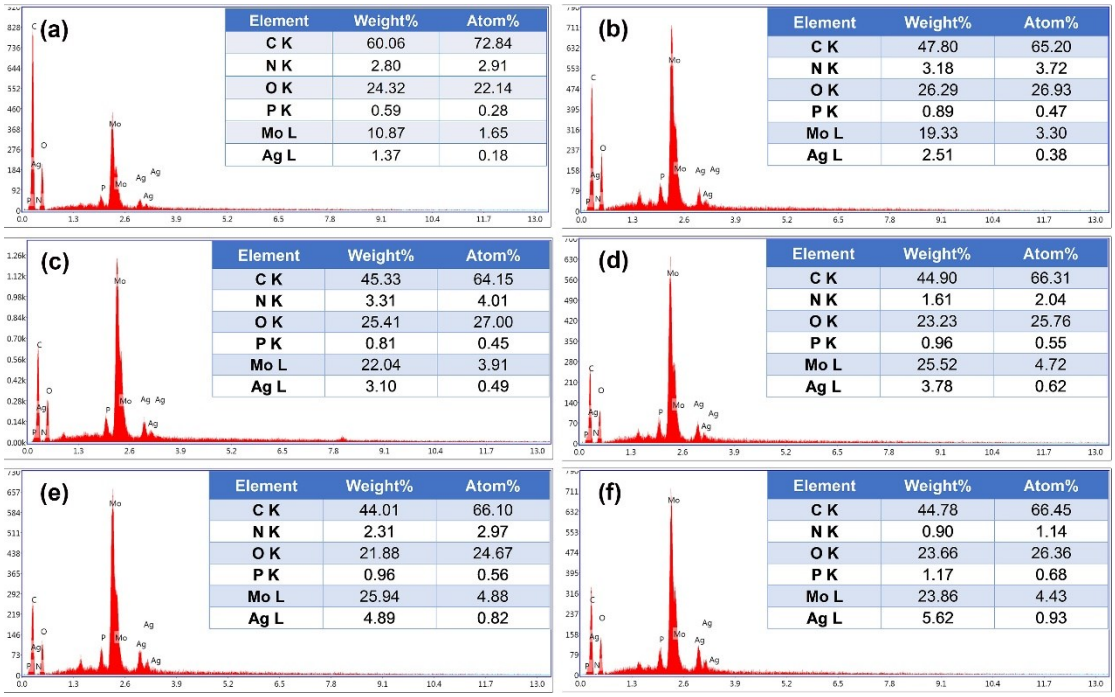

Figure S6. EDX spectra indicate the mass ratios of Ag NPs in Ag/DODA-PMo_{12} composites, (a) 1.37 wt%, (b) 2.51 wt%, (c) 3.10 wt%, (d) 3.78 wt%, (e) 4.89 wt% and (f) 5.62 wt%.

A series of Ag/DODA-PMo_{12} composites with different loading amount of Ag NPs are synthesized by controlling the concentration of AgOA. The Ag/DODA-PMo_{12} composite with Ag NPs content of 1.37 wt%, 2.51 wt%, 3.10 wt%, 3.78 wt%, 4.89 wt% and 5.62wt% are obtained, respectively. The mass ratios of Ag NPs in the composites are measured by the EDX spectrum.

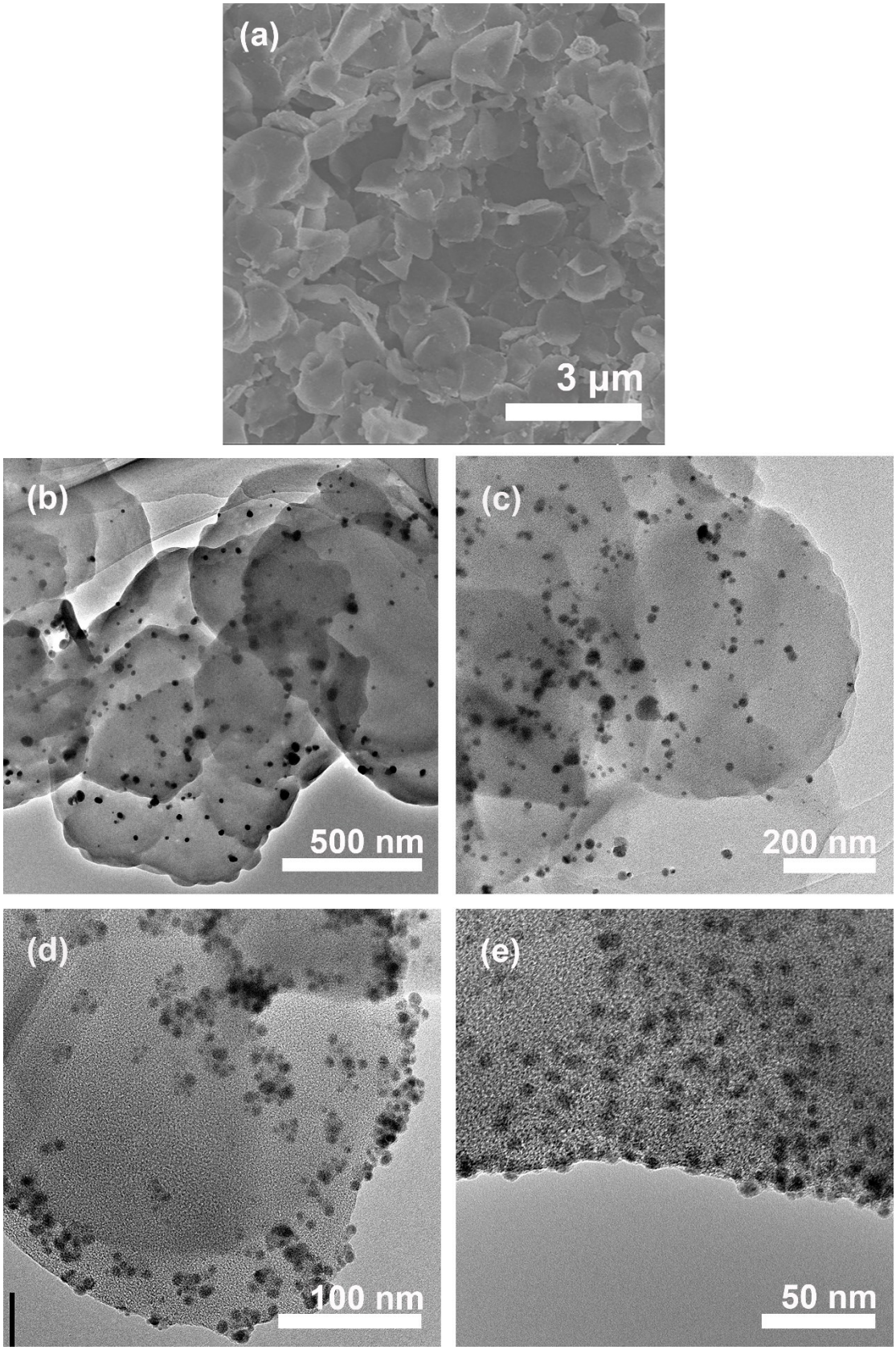

Figure S7. (a) SEM images of Ag/DODA-PMo_{12} composites. TEM images of Ag/DODA-PMo_{12} composites at various visual field: (b) 500 nm, (c) 200 nm, (d) 100 nm and (e) 50 nm.

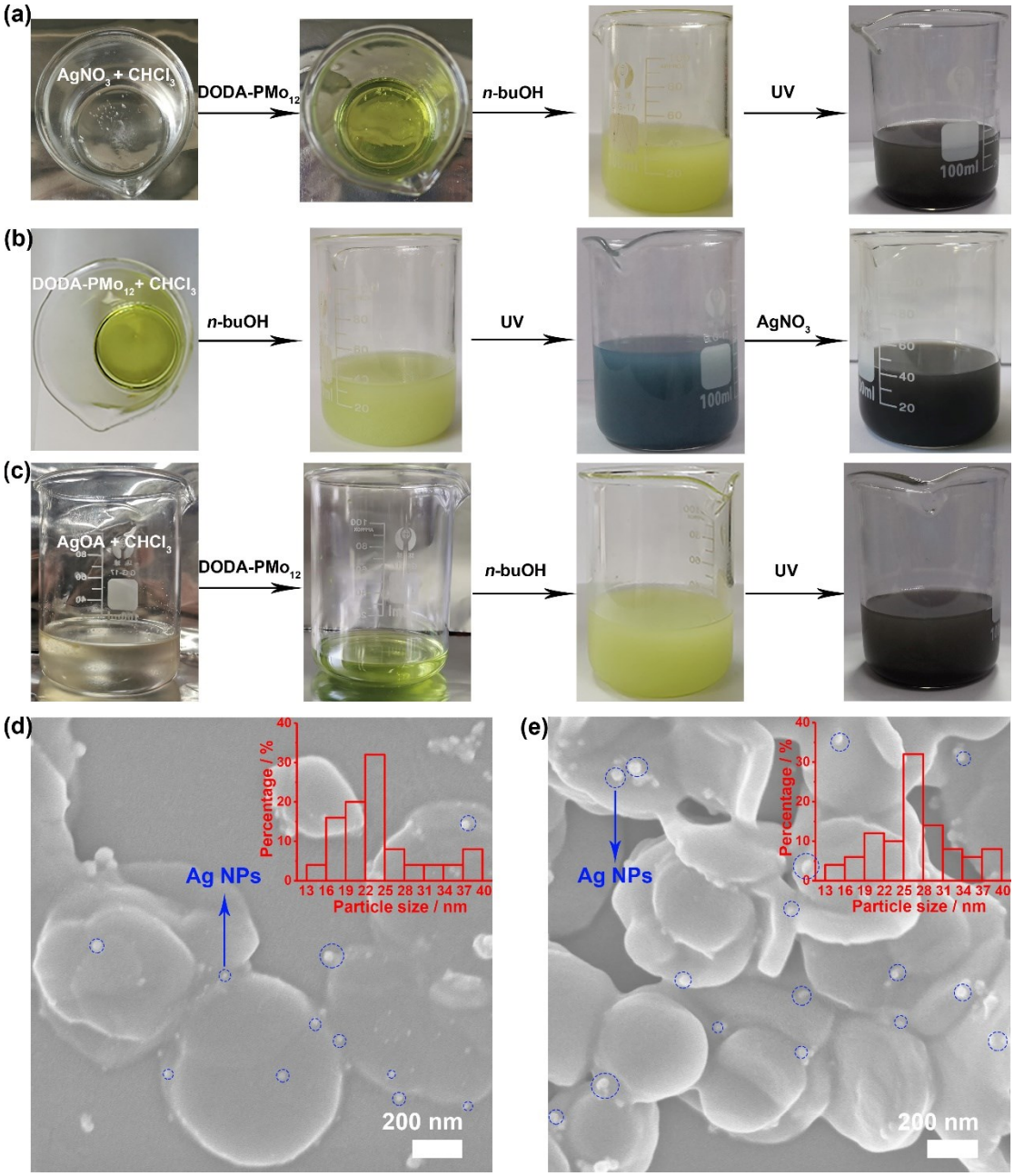

Figure S8. Experimental phenomenon images of the (a) Comparative Sample-**1**, (b) Comparative Sample-**2** and Ag/DODA-PMo_{12}. SEM images of the prepared (d) Comparative Sample-**1** and (e) Comparative Sample-**2** (inset: size distribution of Ag NPs，22±8 nm, 27±13 nm, respectively).

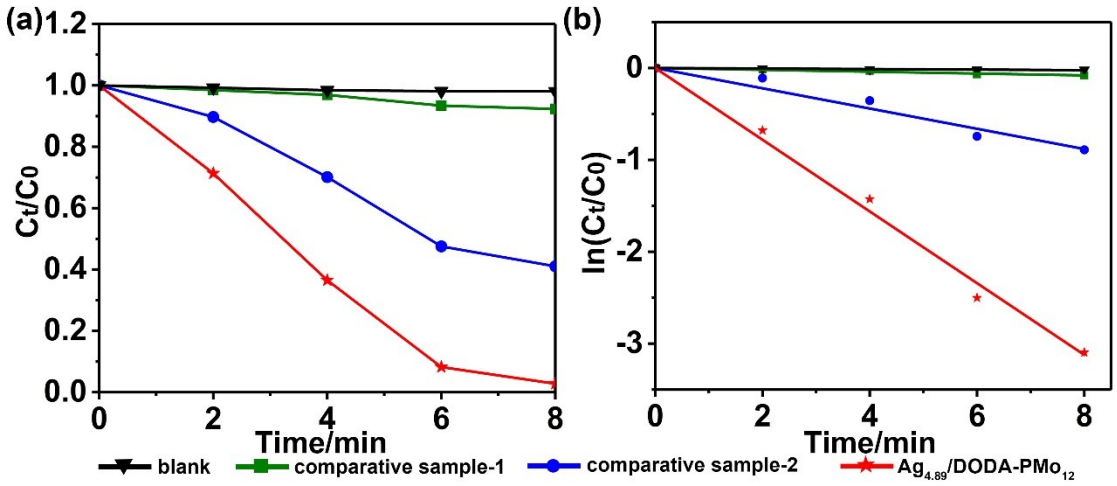

Figure S9. (a) Temporal course of the reduction of 4-NP by Comparative Sample-**1**, Comparative Sample-**2** and $Ag_{4.89}$/DODA-PMo_{12}. (b) Corresponding plots of $\ln(C_t/C_0)$ *vs* time *t* toward the reduction.

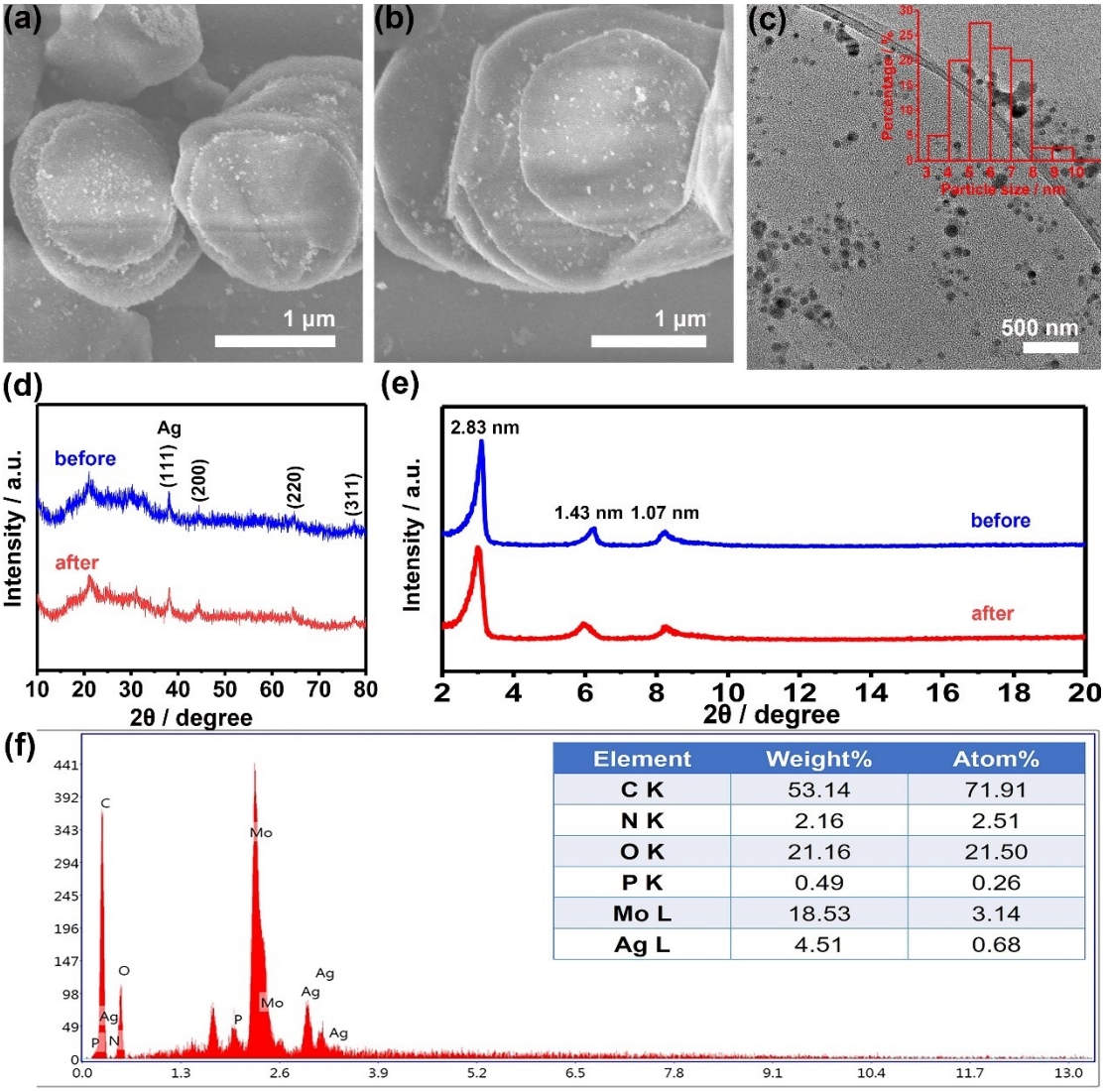

Element	Weight%	Atom%
C K	53.14	71.91
N K	2.16	2.51
O K	21.16	21.50
P K	0.49	0.26
Mo L	18.53	3.14
Ag L	4.51	0.68

Figure S10. SEM images of the $Ag_{4.89}$/DODA-PMo_{12} composite (a) before and (b) after catalytic reaction. (c) TEM images of the $Ag_{4.89}$/DODA-PMo_{12} composite after catalytic reaction (inset: size distribution of Ag NPs，6±2 nm). (d) Wide-angle XRD and (e) Small-angle XRD patterns of $Ag_{4.89}$/DODA-PMo_{12} composite after catalytic reaction. (f) EDX spectrum indicates the mass ratio of Ag NPs in $Ag_{4.89}$/DODA-PMo_{12} composites after catalytic reaction

Table S1. The BE values (eV) and relative areas of components (%) of Mo $3d_{5/2}$ core excitations obtained for Ag/DODA-PMo_{12} and $H_3PMo_{12}O_{40}$.

Sample	Mo $3d_{5/2}$				Mo^{5+}/ Mo^{6+}
	Mo^{5+}		Mo^{6+}		
	BE (eV)	Area (%)	BE (eV)	Area (%)	
Ag/DODA-PMo_{12}	232.23	55.35	232.96	44.65	1.24
$H_3PMo_{12}O_{40}$	—	—	233.08	100	—

Table S2. *k* values of ln (C_t/C_0) *vs* time *t* of catalytic reduction of different samples

Sample	*k* (s^{-1})
$Ag_{4.89}$/DODA-PMo_{12}	**6.49×10^{-3}**
$Ag_{1.37}$/DODA-PMo_{12}	4.11×10^{-4}
$Ag_{2.51}$/DODA-PMo_{12}	6.58×10^{-4}
$Ag_{3.10}$/DODA-PMo_{12}	1.98×10^{-3}
$Ag_{3.78}$/DODA-PMo_{12}	2.28×10^{-3}
$Ag_{5.62}$/DODA-PMo_{12}	1.51×10^{-3}
Comparative Sample-**1**	1.67×10^{-4}
Comparative Sample-**2**	1.84×10^{-3}

Table S3. Comparison of the Ag/DODA-PMo_{12} catalyst with reported catalysts.

Entry	Catalyst	k (s^{-1})	4-NP concentration (mM)	$NaBH_4$ concentration	Reference
1	Ag/CTAB-PW_{12} nanowire	3.15×10^{-3}	0.12	60 mM	S1
2	activated carbon-Ag	6.67×10^{-3}	0.1	0.12 M	S2
3	oxygen-functionalized CNTs-Ag	3.33×10^{-3}	0.1	0.12 M	S2
4	Ag-L NPs/LCG3	6.18×10^{-3}	0.1	10 mM	S3
5	Ag@sulfamide-resin	2.51×10^{-3}	1.25	0.12 M	S4
6	Ag–Au@P(NIPAM-co-MAPTMS)-3	2.9×10^{-3}	2	0.1 M	S5
7	AuAg@pNIPAM	5.7×10^{-3}	0.1	60 mM	S6
8	Au@PGNCS	2.53×10^{-3}	2.5	40 mM	S7
9	Ag^0 /CA-CuO	4.17×10^{-3}	0.15	15 mM	S8
10	Ag/DODA-PMo_{12} nanosheet	6.49×10^{-3}	0.12	60 mM	**This work**

Reference

[S1] W.-Z. Zhou, X.-J. Feng, H.-Q. Tan, H.-F. Shi, Y.-H. Wang, S. Gao, Y.-G. Li, *Chem. Asian J.*, 2016, **11**, 3107–3112.

[S2] L. L. Shui, G. X. Zhang, B. Hu, X. X. Chen, M. L. Jin, G. F. Zhou, N. Li, M. Muhler, B. X. Peng, *J. Energy Chem.*, 2019, **36**, 37-46.

[S3] L. L. Zhang, H. L. Lu, J. J. Chu, J. X. Ma, Y. M. Fan, Z. G. Wang, Y. H. Ni, *ACS Sustain. Chem. Eng.*, 2020, **8**, 12655−12663.

[S4] L. Wang, X. J. Chen, Y. D. Duan, Q. Z. Luo, D. S. Wang, *Catal. Sci. Technol.*, 2020, **10**, 4191-4200.

[S5] L. Li, R. Niu, Y. Zhang, *RSC Adv.*, 2018, **8**, 12428–12438.

[S6] L. Tzounis, M. Dona, J. M. Lopez-Romero, A. Fery, R. Contreras-Caceres, *ACS Appl. Mater. Interfaces*, 2019, **11**, 29360−29372.

[S7] Y. Z. Li, L. Q. Zhu, B. J. Wang, Z. P. Mao, H. Xu, Y. Zhong, L. P. Zhang, X. F. Sui, *ACS Appl. Mater. Interfaces*, 2018, **10**, 27831−27839.

[S8] F. U. Khan, Asimullah, S. B. Khan, T. Kamal, A. M. Asiri, I. U. Khan, K. Akhtar, *Int. J. Biol. Macromol.*, 2017, **102**, 868–877.